OL Organic Letters

pubs.acs.org/OrgLett Letter

6,21-Diaza-*m*-benziporphyrins and 6,21-Diaza-*m*-pyriporphyrins with *meso*-*N*-Substituents: Synthesis and Evaluation of Antiaromatic Characters

Published as part of Organic Letters special issue "π-Conjugated Molecules and Materials".

Emi Suzuki, Momo Kaneko, Haruyuki Nakano, and Yoshihiro Matano*

Cite This: *Org. Lett.* 2025, 27, 8712–8717 Read Online

ACCESS | Metrics & More | Article Recommendations | Supporting Information

ABSTRACT: The first examples of 6,21-diaza-*m*-benziporphyrin (R_2DABP) and 6,21-diaza-*m*-pyriporphyrin (Ph_2DAPP) with methyl or phenyl groups on the *meso* nitrogen atoms, along with new examples of dioxa-*m*-benziporphyrin, are reported. The metal complexes of R_2DABP and Ph_2DAPP exhibit red-shifted optical absorption bands that extend into the near-infrared region, compared to their corresponding freebase forms. NMR spectroscopy reveals that the metalation of the freebase of Ph_2DAPP enhances the paratropic ring-current effect originating from the pseudo 20π-electron macrocyclic pathway.

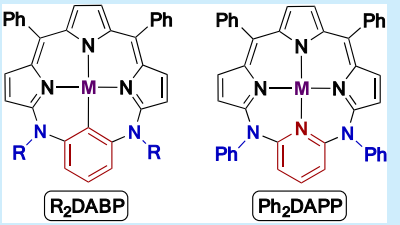

Core modification is a well-established strategy for significantly altering the optical and redox properties and coordination ability of porphyrins.[1] Benziporphyrins and pyriporphyrins, in which one of the pyrrole rings of the porphyrin is replaced by a benzene ring and a pyridine ring, respectively, represent prominent examples that have been extensively studied by several groups (Figure 1).[2−5] A central focus of the study was to understand the relationship between molecular structure and aromaticity in these core-modified porphyrins. For example, Latos-Grażyński et al. synthesized *m*-benziporphyrin **P1** and *m*-pyriporphyrin **P2** and evaluated their aromatic characters using NMR spectroscopy.[2] Consequently, the freebase forms of **P1** and **P2** were found to be intrinsically nonaromatic, whereas a Zn^{II} complex and the protonated freebase of **P2** exhibited diamagnetic ring-current effects that suggested the coexistence of an 18e-macrocyclic π-delocalization pathway with the pyridine [6]annulene circuit. Lash et al. demonstrated that oxybenziporphyrins and oxypyriporphyrins are aromatic, with 18π-electron chlorin-like conjugation pathways.[3] Recently, benziporphyrins modified with *meso*-nitrogen atoms have also been reported. Osuka et al. synthesized 6,21-diaza-6,21-dihydro-*m*-benziporphyrin **P3**, which contains two additional π electrons compared to **P1**, and concluded that it exhibits nonaromatic character based on both experimental and theoretical results.[6] By contrast, Uchiyama et al. synthesized the isoelectronic tetraaza-*m*-benziporphyrin **P4** and concluded that it is antiaromatic, and exhibits a weak paratropic ring current originating from a pseudo 20π-electron pathway.[7] These studies highlighted that the degree of aromatic or antiaromatic character in benziporphyrins, pyriporphyrins, and their aza analogs is extremely sensitive to their molecular components. However, no information is available on the effect of *meso*-*N*-substituents on the antiaromaticity of azabenziporphyrin and azapyriporphyrin derivatives.

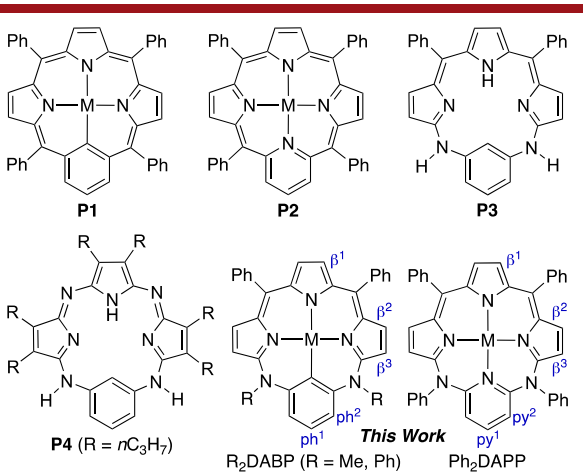

Figure 1. Structures of **P1**, **P2**, **P3**, **P4**, R_2DABP, and Ph_2DAPP. M = H_2/H, Pd^{II}, Ni^{II}, Zn^{II}, etc.

We have shown that 20π-electron 5,10,15,20-tetraaryl-5,15-diazaporphyrinoids (Ar_4DAP) are remarkably air-stable compared to the isoelectronic 5,10,15,20-tetraarylporphyrin

Received: June 26, 2025
Revised: July 18, 2025
Accepted: July 22, 2025
Published: July 25, 2025

https://doi.org/10.1021/acs.orglett.5c02644
Org. Lett. 2025, 27, 8712–8717

dianions.[8] This characteristic property of Ar_4DAP makes it a promising research subject for elucidating the structure–property relationships of antiaromatic azaporphyrins.[9,10] For instance, NMR studies on the six-coordinate tin(IV) complexes of Ar_4DAP have revealed that the paramagnetic ring-currents originating from the 20π-electron diazaporphyrin ring increase with a decrease in energy gaps between the highest occupied molecular orbital (HOMO) and lowest unoccupied molecular orbital (LUMO).[10] Herein, we report the first examples of 6,21-diaza-*m*-benziporphyrins and 6,21-diaza-*m*-pyriporphyrin with methyl or phenyl groups on the *meso* nitrogen atoms (designated as R_2DABP and Ph_2DAPP, respectively; R = Me or Ph. Figure 1), along with new examples of isoelectronic 6,21-dioxa-*m*-benziporphyrin (DOBP), studied in their freebases and metal complexes. In addition to the optical and redox properties of these *meso*-heteroporphyrinoids, the effects of the *meso* heteroatoms, *N*-substituents, and central metals on the paramagnetic ring-current effects arising from the pseudo 20π-electron pathways were evaluated based on the experimental and theoretical results.

Scheme 1 depicts the synthesis of freebases, Me_2DABP **2H$_2$**, Ph_2DABP **3H$_2$**, and Ph_2DAPP **4H**. Treatment of α,α'-dibromotripyrrin **1**[11] with *N*,*N*′-dimethyl-1,3-phenylenediamine[12] in boiling THF for 28 h afforded Me_2DABP **2H$_2$** in 60% yield. Buchwald–Hartwig C–N cross-coupling between dibromotripyrrin **1** and *N*,*N*′-diphenyl-1,3-phenylenediamine[13] under the reaction conditions mentioned in Scheme 1 afforded Ph_2DABP **3H$_2$** in 53% yield. Under the same reaction conditions, dibromotripyrrin **1** underwent C–N cross-coupling with N^2,N^6-diphenyl-2,6-pyridinediamine[14] to afford Ph_2DAPP **4H** in 32% yield.

Scheme 1. Synthesis of Freebases 2H$_2$, 3H$_2$, and 4H

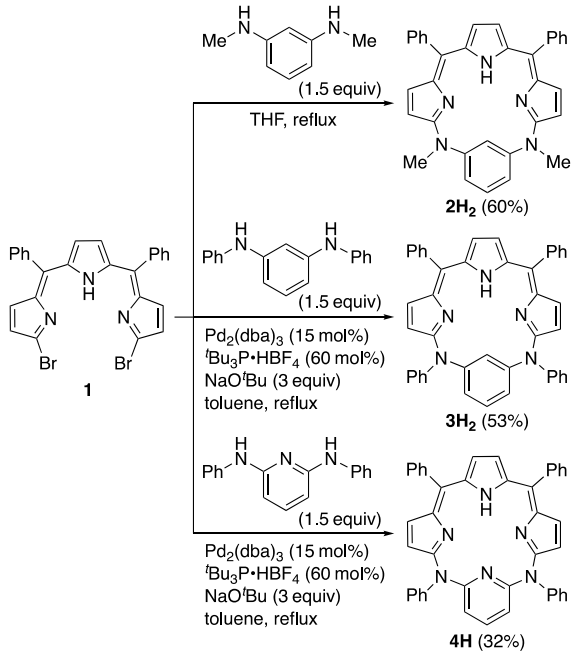

The complexation reactions of the freebases with metal(II) salts are summarized in Scheme 2. Me_2DABP **2H$_2$** and Ph_2DABP **3H$_2$** reacted with $Pd(OAc)_2$ in chlorobenzene at 110 °C to furnish the corresponding Pd^{II} complexes **2Pd** and **3Pd** in 93–95% yields. The complexation of **3H$_2$** with $NiCl_2$ in boiling acetonitrile produced Ni^{II} complex **3Ni** via similar C–H activation. Ph_2DAPP **4H** underwent complexation with $Pd(OAc)_2$ in acetonitrile to yield the cationic Pd^{II} complex **4Pd** after anion exchange with KPF_6. Ph_2DAPP **4H** also reacted with $ZnCl_2$ in the presence of K_2CO_3 in CH_2Cl_2 at room temperature to yield Zn^{II} complex **4Zn**.

Scheme 2. Synthesis of Metal Complexes 2Pd, 3M, and 4M

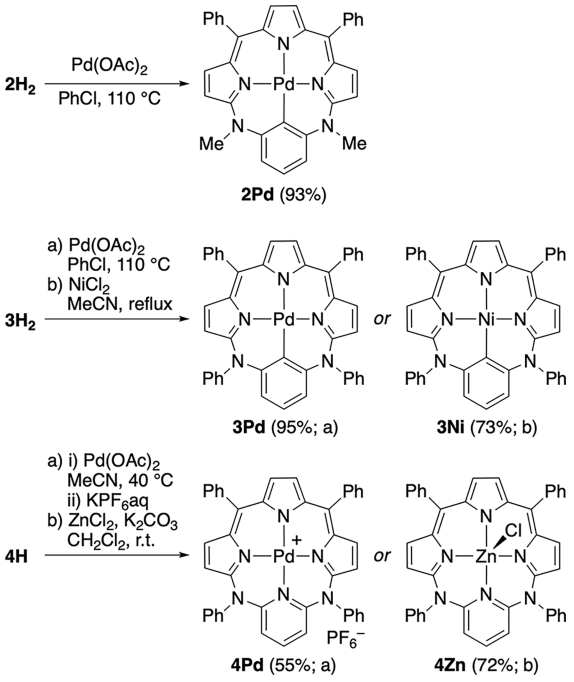

To investigate the influence of the two *meso*-heteroatoms on the fundamental properties of *m*-benziporphyrins, new DOBP derivatives **5H$_2$**, **5Pd**, and **5Ni** (Figure 2) were prepared according to a previously reported methodology[15] (for details, see the Supporting Information).

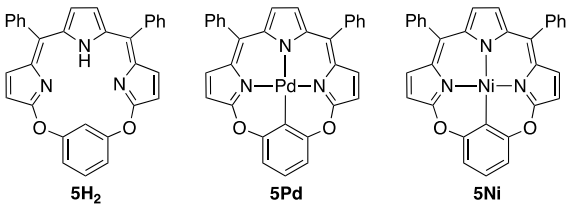

Figure 2. Structures of DOBP derivatives **5H$_2$**, **5Pd**, and **5Ni**.

New *meso*-heteroporphyrinoids **2M**, **3M**, **4M**, and **5M** were isolated as air-stable solids and characterized using NMR spectroscopy and high-resolution electrospray ionization mass spectrometry. Attempts to grow single crystals of these compounds were unsuccessful. The salient features of the ^{1}H NMR spectra are discussed below. The optical and redox properties of **2M**, **3M**, **4M**, and **5M** in CH_2Cl_2 were investigated using ultraviolet–visible–near-infrared (UV–vis–NIR) absorption spectroscopy and cyclic voltammetry (CV). The results are illustrated in Figures 3, 4, and S1. In the UV–vis–NIR absorption spectra of the R_2DABP derivatives, the freebases **2H$_2$** and **3H$_2$** exhibited intense bands in the wavelength range of 500–700 nm, whereas the Pd^{II} complexes **2Pd** and **3Pd** exhibited significantly red-shifted absorption bands in the range of 600–850 nm (Figures 3a,b). Similarly,

https://doi.org/10.1021/acs.orglett.5c02644
Org. Lett. 2025, 27, 8712–8717

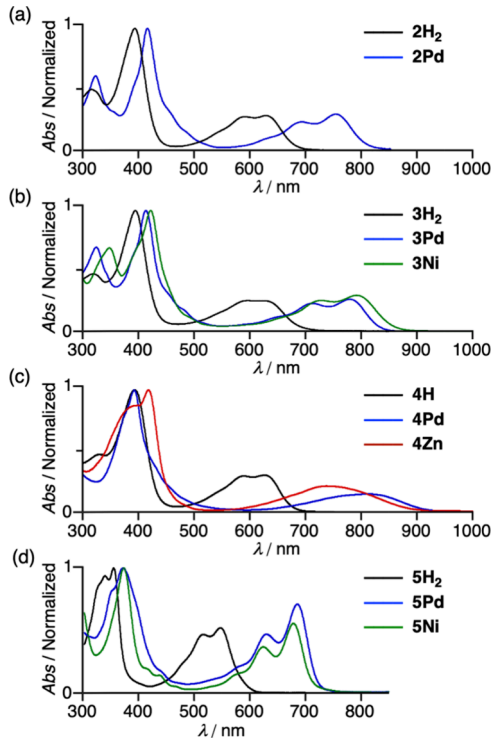

Figure 3. Normalized UV−vis−NIR absorption spectra of (a) **2M**, (b) **3M**, (c) **4M**, and (d) **5M** in CH_2Cl_2.

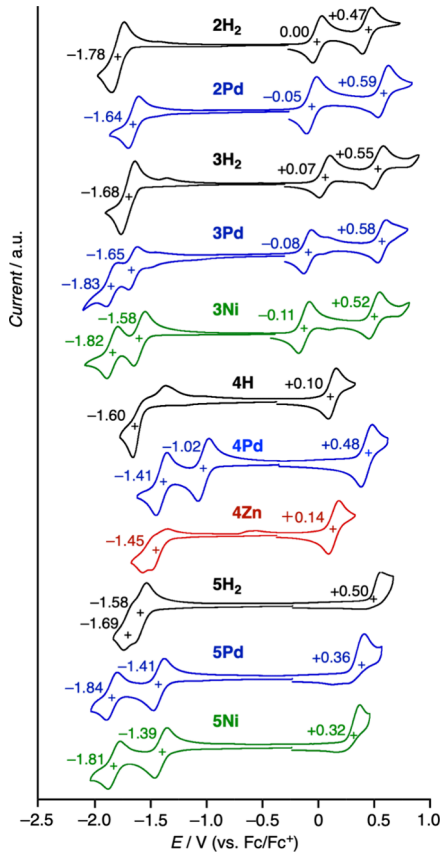

Figure 4. Cyclic voltammograms and redox potentials vs ferrocene/ferrocenium (Fc/Fc^+) of **2M**, **3M**, **4M**, and **5M** in CH_2Cl_2 with Bu_4NPF_6: scan rate = 60 mV/s. The half-wave potentials are indicated for the reversible processes. The redox potentials of the irreversible processes were determined by differential pulse voltammetry.

the absorption bands of the Pd^{II} complexes **4Pd** and **5Pd** were significantly red-shifted from those of the freebases **4H** and $\mathbf{5H_2}$ (Figures 3c,d). These data indicated that the HOMO−LUMO gaps of the metal complexes were significantly narrower than those of the corresponding freebases. The spectral features and absorption maxima (λ_{max}) of R_2DABP were largely unaffected by differences in the *meso*-*N*-substituents (Me vs Ph) and central metals (Pd vs Ni). By contrast, there was a large difference in the λ_{max} values between the Ph_2DABP derivatives **3M** (λ_{max} = 780−792 nm; M = Pd, Ni) and DOBP derivatives **5M** (λ_{max} = 679−685 nm; M = Pd, Ni). This difference can be attributed to the comparatively lower stability of the HOMO in **3M** relative to that in **5M** (vide infra). The longest λ_{max} values of **3M** and **4M** are blue-shifted from those reported for **P1** (λ_{max} = 723 nm for M = H_2, 875 nm for M = Pd)[2a] and **P2** (λ_{max} = 685 nm for M = H, 848 nm for M = ZnCl),[2d] respectively, reflecting the difference in the number of all π-electrons in their macrocycles. DOBP freebase $\mathbf{5H_2}$ and Pd^{II} complex **5Pd** were fluorescent (Figure S1), as observed for analogous derivatives with *meso*-C_6F_5 groups,[15] whereas DABP and DAPP derivatives $\mathbf{2H_2}$, $\mathbf{3H_2}$, and **4H** were nonfluorescent.

Density functional theory (DFT) calculations were performed to gain some insight into the molecular structures and origins of the electronic transitions of **2M**, **3M**, and **4M**. As shown in Figures S2, S3, and S4, the HOMO and LUMO are mainly located in the tripyrrin unit. Metalation improves the overall planarity of the macrocycle, as inferred from a decrease in the dihedral angles at the *meso*-N bridges, from 56.6°−68.2° to 22.0°−43.3°. The metal coordination-induced planarization thereby increased the degree of π-conjugation between the tripyrrin and benzene/pyridine units and dπ−pπ orbital interactions for the Pd^{II} complexes. Time-dependent DFT (TD-DFT) calculations revealed that the lowest excited state is composed almost entirely of a HOMO to LUMO π−π* transition and that the metalation reduces the electronic transition energies (Table S1).

Figure 4 summarizes the cyclic voltammograms of **2M**, **3M**, **4M**, and **5M**. In contrast to **P3**, both $\mathbf{2H_2}$ and $\mathbf{3H_2}$ exhibited reversible redox couples for all processes, indicating that the *meso*-*N*-methyl and *meso*-*N*-phenyl substituents provided electrochemical stability to the oxidized and reduced DABP species. The influence of the *N*-substituents on the redox potentials of R_2DABP falls within the range of 0.01−0.10 V. Notably, metalation with Pd^{II} caused a shift in the first oxidation and reduction processes of the R_2DABP chromophores to the negative and positive sides, respectively, thus decreasing their electrochemical HOMO−LUMO gaps by 0.18−0.19 V. This explains the results obtained by UV−vis−NIR absorption spectroscopy and DFT calculations (vide supra). In addition, metalation of **4H** and $\mathbf{5H_2}$ with Pd^{II}, Zn^{II}, and Ni^{II} salts resulted in narrowing of the HOMO−LUMO gaps of the Ph_2DAPP and DOBP chromophores. The Ph_2DABP derivatives, **3M**, were easily oxidized and more difficult to reduce than the corresponding DOBP derivatives, **5M**, clearly reflecting the differing electronic effects of the *meso* heteroatom units on the HOMO and LUMO energies. The redox potentials of Pd^{II} complex **4Pd** are shifted to the positive side by 0.38−0.58 V relative to those of freebase **4H**, which reflects the cationic character of the Ph_2DAPP chromophore of **4Pd**.

https://doi.org/10.1021/acs.orglett.5c02644
Org. Lett. 2025, 27, 8712−8717

Possible paramagnetic ring-current effects originating from the *meso*-heteroporphyrinoids was evaluated with the aid of NMR spectroscopy. Selected regions of the ^{1}H NMR spectra of **2M**, **3M**, **4M**, and **5M** are depicted in Figures 5 and S5.

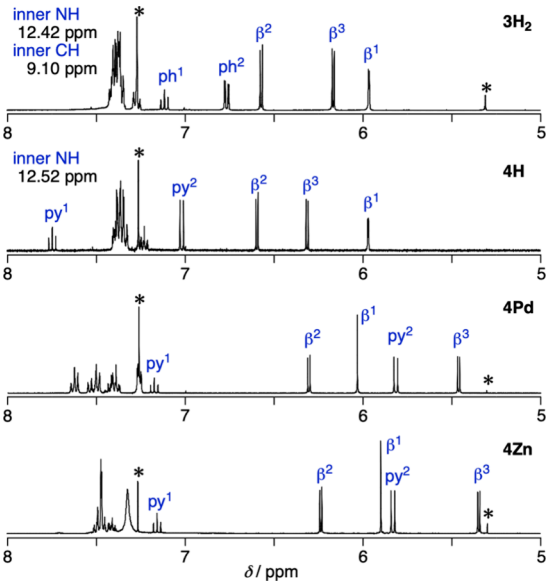

Figure 5. Selected regions (8−5 ppm) of the ^{1}H NMR spectra of $\mathbf{3H_2}$ and **4M** (400 MHz, $CDCl_3$). Asterisks indicate residual solvent peaks. See Figure 1 for the abbreviation of peripheral positions.

Freebases $\mathbf{2H_2}$, $\mathbf{3H_2}$, **4H**, and $\mathbf{5H_2}$ exhibited three types of pyrrolic β-CH signals in the range of 6.70−5.93, 6.57−5.96, 6.59−5.97, and 6.68−5.97 ppm, respectively, suggesting the intrinsically nonaromatic or weakly antiaromatic nature. Nuclear independent chemical shift (NICS)[16] values calculated at the center of the macrocycles of $\mathbf{2H_2}$ (+2.13 ppm), $\mathbf{3H_2}$ (+2.23 ppm), and **4H** (+1.59 ppm) supported their very weak antiaromaticity (Table S2). The deshielded appearance of the inner NH/CH signals of $\mathbf{2H_2}$ (12.14/8.81 ppm), $\mathbf{3H_2}$ (12.42/9.10 ppm), and **4H** (12.52 ppm) may be primarily due to the intramolecular hydrogen bonding interactions between the NH/CH groups and lone pairs located on nitrogen. The effects of metalation on the peripheral CH signals of R_2DABP and DOBP are complex (Figure S5). Metalation basically narrows the dihedral angles at the *meso* heteroatoms, consequently enhancing the degree of π-conjugation. However, the chemical shifts of the peripheral CH signals of **2M**, **3M**, and **5M** do not clearly show an increase in the paramagnetic ring-current effect arising from pseudo 20π-electron pathways of their macrocyclic scaffolds. By contrast, most of the peripheral CH signals of the Ph_2DAPP ring shifted upfield upon metalation (Figure 5). For example, the β^3-CH and py^2-CH signals of **4Zn** observed at 5.35 and 5.83 ppm, respectively, were shifted upfield by 0.96−1.19 ppm from the corresponding signals of **4H**. The metalation is likely to enhance the contribution of the paramagnetic ring-current effect originating from the pseudo 20π-electron circuit of Ph_2DAPP ligand. As mentioned in the Introduction, Latos-Grażyński et al. reported that metalation and protonation of the freebase of **P2** (M = H_2) highlighted the coexistence of a single 18e-macrocyclic π-delocalization pathway with the [6]annulene aromaticity of the pyridine unit.[2] By contrast, the present findings suggest that the 20e-macrocyclic π-delocalization pathway, represented as canonical form **4M-C** in Scheme 3, should be considered along

Scheme 3. Resonance Structures of 4M

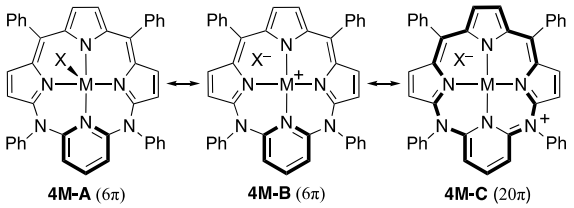

with **4M-A** and **4M-B** to explain the observed upfield shifts of the peripheral CH signals of **4M**. This was further supported by the relatively positive NICS values (+3.75, +3.21 ppm) calculated at four positions inside the macrocyclic ring of **4Zn** and a slight decrease in the NICS value at the center of the pyridine ring from −8.49 ppm (for **4H**) to −7.04 ppm (for **4Zn**). The antiaromatic nature of **4Zn** was further supported by the anisotropy of the induced current density (ACID) plot,[17] showing a contribution of the paratropic ring current (Figure S6). Therefore, these findings highlight the coexistence of a 20e-macrocyclic π-delocalization pathway with the local [6]annulene aromaticity in **4M** (M = Pd and Zn).[18] It is likely that the metal coordination enhances the antiaromaticity of the 20π-conjugated pathway owing to the increased π-conjugation and decreased HOMO−LUMO gap of the macrocyclic Ph_2DAPP ligand in the case of **4M**.[18]

In summary, the first examples of DABP and DAPP with methyl or phenyl groups on the *meso* nitrogen atoms, along with new examples of DOBP, were synthesized by C−X (X = N, O) bond-forming annulation reactions. All resulting freebases reacted with Pd^{II}, Ni^{II}, and Zn^{II} salts to afford the corresponding metal complexes. Metalation narrowed the HOMO−LUMO gaps of these *meso*-heteroporphyrinoid ligands and significantly red-shifted the longest wavelength absorption bands into the NIR region. Notably, the ^{1}H NMR spectra of the metal complexes of Ph_2DAPP exhibited the peripheral CH signals in the shielded region compared to the corresponding signals of the freebase. This indicated an enhanced contribution of the paramagnetic ring-current originating from the 20π-electron pathway represented as one of the canonical structures. The present study not only elucidates the optical and redox properties of DABP and DAPP derivatives with *meso*-*N*-substituents, but also provides valuable information regarding the structure−antiaromaticity relationship of core-modified azaporphyrinoids.

■ ASSOCIATED CONTENT

Data Availability Statement

The data underlying this study are available in the published article and its Supporting Information.

Supporting Information

The Supporting Information is available free of charge at https://pubs.acs.org/doi/10.1021/acs.orglett.5c02644.

Additional results, experimental procedures, and characterization data (PDF)

■ AUTHOR INFORMATION

Corresponding Author

Yoshihiro Matano − *Department of Chemistry, Faculty of Science, Niigata University, Nishi-ku, Niigata 950-2181, Japan*; Email: matano@chem.sc.niigata-u.ac.jp

https://doi.org/10.1021/acs.orglett.5c02644
Org. Lett. 2025, 27, 8712−8717

Authors

Emi Suzuki − *Department of Fundamental Sciences, Graduate School of Science and Technology, Niigata University, Nishi-ku, Niigata 950-2181, Japan*

Momo Kaneko − *Department of Fundamental Sciences, Graduate School of Science and Technology, Niigata University, Nishi-ku, Niigata 950-2181, Japan*

Haruyuki Nakano − *Department of Chemistry, Graduate School of Science, Kyushu University, Nishi-ku, Fukuoka 819-0395, Japan;* orcid.org/0000-0002-7008-0312

Complete contact information is available at: https://pubs.acs.org/10.1021/acs.orglett.5c02644

Notes

The authors declare no competing financial interest.

■ ACKNOWLEDGMENTS

This work was supported by JSPS KAKENHI (Grant Numbers: 23K23329 to Y.M., 21K04980 to H.N.). We thank Professor Tomohiro Higashino (Kyoto University) for his assistance with mass spectrometry.

■ REFERENCES

(1) (a) Latos-Grażyński, L.; Chmielewski, P. J. Core-modified porphyrins and their nickel complexes: synthesis, characterization, and chemistry. *New J. Chem.* **1997**, *21*, 691−700. (b) Furuta, H.; Maeda, H.; Osuka, A. Confusion, inversion, and creation-a new spring from porphyrin chemistry. *Chem. Commun.* **2002**, *17*, 1795−1804. (c) Chmielewski, P. J.; Latos-Grażyński, L. Core modified porphyrins - a macrocyclic platform for organometallic chemistry. *Coord. Chem. Rev.* **2005**, *249*, 2510−2533. (d) Matano, Y.; Nakabuchi, T.; Imahori, H. Synthesis, structures, and aromaticity of phosphole-containing porphyrins and their metal complexes. *Pure Appl. Chem.* **2010**, *82*, 583−593. (e) Lash, T. D. Carbaporphyrinoid Systems. *Chem. Rev.* **2017**, *117*, 2313−2446. (f) Chatterjee, T.; Shetti, V. S.; Sharma, R.; Ravikanth, M. Heteroatom-Containing Porphyrin Analogues. *Chem. Rev.* **2017**, *117*, 3254−3328. (g) Pushpanandan, P.; Ravikanth, M. Synthesis and Properties of Stable 20π Porphyrinoids. *Chem. Rec.* **2022**, *22*, No. e202200144.

(2) (a) Stepień, M.; Latos-Grażyński, L. Tetraphenylbenziporphyrin-A Ligand for Organometallic Chemistry. *Chem.—Eur. J.* **2001**, *7*, 5113−5117. (b) Stepień, M.; Latos-Grażyński, L.; Szterenberg, L.; Panek, J.; Latajka, Z. Cadmium(II) and Nickel(II) Complexes of Benziporphyrins. A Study of Weak Intramolecular Metal-Arene Interactions. *J. Am. Chem. Soc.* **2004**, *126*, 4566−4580. (c) Stepień, M.; Latos-Grażyński, L. Benziporphyrins: Exploring Arene Chemistry in a Macrocyclic Environment. *Acc. Chem. Res.* **2005**, *38*, 88−98. (d) Mysliborski, R.; Latos-Grazynski, L.; Szterenberg, L. Pyriporphyrin - A Porphyrin Homologue Containing A Built-in Pyridine Moiety. *Eur. J. Org. Chem.* **2006**, *2006*, 3064−3068.

(3) (a) Lash, T. D.; Chaney, S. T.; Richter, D. T. Conjugated Macrocycles Related to the Porphyrins. 12. Oxybenzi- and Oxypyriporphyrins: Aromaticity and Conjugation in Highly Modified Porphyrinoid Structures. *J. Org. Chem.* **1998**, *63*, 9076−9088. (b) Lash, T. D.; Pokharel, K.; Serling, J. M.; Yant, V. R.; Ferrence, G. M. Aromatic and Nonaromatic Pyriporphyrins. *Org. Lett.* **2007**, *9*, 2863−2866. (c) Lash, T. D. Benziporphyrins, a unique platform for exploring the aromatic characteristics of porphyrinoid systems. *Org. Biomol. Chem.* **2015**, *13*, 7846−7878.

(4) Das, M.; Srinivasan, A. Advent and features of pyriporphyrinoids: an overview of a pyridine-based porphyrin analogue. *Chem. Commun.* **2023**, *59*, 11780−11790.

(5) (a) Liu, L.; Zhang, F.; Xu, L.; Zhou, M.; Yin, B.; Tanaka, T.; Osuka, A.; Song, J. *m*-Benziporphyrin(1.1.0.0)s as a Rare Example of Ring-Contracted Carbaporphyrins with Metal-Coordination Ability: Distorted Coordination Structures and Small HOMO-LUMO Gaps. *Chem.—Eur. J.* **2023**, *29*, No. e202203517. (b) Liu, L.; Song, S.; Lee, J.; Rao, Y.; Xu, L.; Zhou, M.; Yin, B.; Oh, J.; Kim, J.; Osuka, A.; Song, J. Sub-*m*-benziporphyrin: a subcarbaporphyrinoid and its B^{III} complex with an unprecedented planar tridentate 14π-aromatic network. *Chem. Sci.* **2025**, *16*, 1155−1160.

(6) Umetani, M.; Tanaka, T.; Osuka, A. Synthesis of azabenziporphyrinoids by S_NAr reactions. *J. Porphyr. Phthalocyanines* **2020**, *24*, 794−801.

(7) (a) Yanagi, S.; Matsumoto, A.; Toriumi, N.; Tanaka, Y.; Miyamoto, K.; Muranaka, A.; Uchiyama, M. A Switchable Near-Infrared-Absorbing Dye Based on Redox-Bistable Benzitetraazaporphyrin. *Angew. Chem., Int. Ed.* **2023**, *62*, No. e202218358. (b) Yanagi, S.; Takayama, O.; Toriumi, N.; Muranaka, A.; Hashizume, D.; Uchiyama, M. 20π-Electron Antiaromatic Benziphthalocyanines with Absorption Reaching the Near-Infrared-II Region. *Chem.—Eur. J.* **2024**, *30*, No. e202400401.

(8) (a) Satoh, T.; Minoura, M.; Nakano, H.; Furukawa, K.; Matano, Y. Redox-Switchable 20π-, 19π-, and 18π-Electron 5,10,15,20-Tetraaryl-5,15-diazaporphyrinoid Nickel(II) Complexes. *Angew. Chem., Int. Ed.* **2016**, *55*, 2235−2238. (b) Sudoh, K.; Satoh, T.; Amaya, T.; Furukawa, K.; Minoura, M.; Nakano, H.; Matano, Y. Syntheses, Properties, and Catalytic Activities of Metal(II) Complexes and Free Bases of Redox-Switchable 20π, 19π, and 18π 5,10,15,20-Tetraaryl-5,15-diazaporphyrinoids. *Chem.—Eur. J.* **2017**, *23*, 16364−16373. (c) Satoh, Y.; Kudoh, Y.; Furukawa, K.; Matano, Y. Synthesis, Electrochemical Behavior, and Catalytic Activity of Cobalt Complexes of 5,10,15,20-Tetraaryl-5,15-diazaporphyrinoids. *Org. Lett.* **2022**, *24*, 3839−3843. (d) Matano, Y. Recent Advances in the Synthesis of Diazaporphyrins and Their Chalcogen Derivatives. *Org. Biomol. Chem.* **2023**, *21*, 3034−3056.

(9) Ochiai, H.; Furukawa, K.; Nakano, H.; Matano, Y. Doubly Strapped Redox-Switchable 5,10,15,20-Tetraaryl-5,15-diazaporphyrinoids: Promising Platforms for the Evaluation of Paratropic and Diatropic Ring-Current Effects. *J. Org. Chem.* **2021**, *86*, 2283−2296.

(10) Suzuki, H.; Minoura, M.; Furukawa, K.; Nakano, H.; Matano, Y. Sn(IV) Complexes of 5,10,15,20-Tetraaryl-5,15-diazaporphyrinoids: A Promising Platform for Evaluating the 20π-Electron Antiaromaticity. *Chem.—Eur. J.* **2025**, *31*, No. e202404092.

(11) Umetani, M.; Tanaka, T.; Osuka, A. Conjugated double helices via self-dimerization of α,α'-dianilinotripyrrins. *Chem. Sci.* **2018**, *9*, 6853−6859.

(12) Redko, B.; Albeck, A.; Gellerman, G. Facile synthesis and antitumor activity of novel *N*(9) methylated AHMA analogs. *New J. Chem.* **2012**, *36*, 2188−2191.

(13) (a) Zhang, K.; Wang, X.; Chang, Y.; Wu, Y.; Wang, S.; Wang, L. Carbazole-Decorated Organoboron Emitters with Low-Lying HOMO Levels for Solution-Processed Narrowband Blue Hyperfluorescence OLED Devices. *Angew. Chem., Int. Ed.* **2023**, *62*, No. e202313084. (b) Wei, J.; Shi, J.; Ni, R.; Huang, D. A novel group of *N,N*-diaryl-1,2-benzenediamine room temperature phosphors based on structural engineering. *Dyes Pigments* **2024**, *225*, 112104.

(14) Wagaw, S.; Buchwald, S. L. The Synthesis of Aminopyridines: A Method Employing Palladium-Catalyzed Carbon-Nitrogen Bond Formation. *J. Org. Chem.* **1996**, *61*, 7240−7241.

(15) Zhang et al. reported DOBP derivatives with *meso*-C_6F_5 groups: (a) Yao, Y.; Hou, C.-L.; Yang, Z.-S.; Ran, G.; Kang, L.; Li, C.; Zhang, W.; Zhang, J.; Zhang, J.-L. Unusual near infrared (NIR) fluorescent palladium(II) macrocyclic complexes containing M-C bonds with bioimaging capability. *Chem. Sci.* **2019**, *10*, 10170−10178. (b) Yao, Y.; Ran, G.; Hou, C.-L.; Zhang, R.; Mangel, D. N.; Yang, Z.-S.; Zhu, M.; Zhang, W.; Zhang, J.; Sessler, J. L.; Gao, S.; Zhang, J.-L. Nonaromatic Organonickel(II) Phototheranostics. *J. Am. Chem. Soc.* **2022**, *144*, 7346−7356.

(16) (a) Schleyer, P. v. R.; Maerker, C.; Dransfeld, A.; Jiao, H.; van Eikema Hommes, N. J. R. Nucleus-Independent Chemical Shifts: A Simple and Efficient Aromaticity Probe. *J. Am. Chem. Soc.* **1996**, *118*, 6317−6318. (b) Chen, Z.; Wannere, C. S.; Corminboeuf, C.; Puchta, R.; Schleyer, P. v. R. Nucleus-Independent Chemical Shifts (NICS) as

an Aromaticity Criterion. *Chem. Rev.* **2005**, *105*, 3842−3888 and references therein.
(17) Geuenich, D.; Hess, K.; Köhler, F.; Herges, R. Anisotropy of the Induced Current Density (ACID), a General Method To Quantify and Visualize Electronic Delocalization. *Chem. Rev.* **2005**, *105*, 3758−3772.
(18) Latos-Grażyński et al. reported switching of antiaromaticity of 22-hydroxybenziporphyrin by phenol-keto tautomerization; a keto form exhibited a [20]annulenoid structure characterized by macrocyclic antiaromaticity. See: Stepień, M.; Latos-Grażyński, L.; Szterenberg, L. 22-Hydroxybenziporphyrin: Switching of Antiaromaticity by Phenol-Keto Tautomerization. *J. Org. Chem.* **2007**, *72*, 2259−2270.

https://doi.org/10.1021/acs.orglett.5c02644
Org. Lett. 2025, 27, 8712−8717